frontiers | Frontiers in Materials

TYPE Original Research
PUBLISHED 27 September 2022
DOI 10.3389/fmats.2022.991018

OPEN ACCESS

EDITED BY
Yanjin Lu,
Fujian Institute of Research on the Structure of Matter (CAS), China

REVIEWED BY
Longgang Wang,
Yanshan University, China
Xu Chen,
China Medical University, China
Wei Zheng,
Fujian Institute of Research on the Structure of Matter (CAS), China

*CORRESPONDENCE
Shenghui Su,
sushenghui27@163.com
Jiuzao Lin,
gykndsyy@163.com
Xiaoyong Wang,
wxyong1999@163.com

SPECIALTY SECTION
This article was submitted to Biomaterials and Bio-Inspired Materials, a section of the journal Frontiers in Materials

RECEIVED 11 July 2022
ACCEPTED 15 August 2022
PUBLISHED 27 September 2022

CITATION
Zhou C, Su S, Fan J, Lin J and Wang X (2022), Engineered electrospun poly(lactic-co-glycolic acid)/Si_3N_4 nanofiber scaffold promotes osteogenesis of mesenchymal stem cell.
Front. Mater. 9:991018.
doi: 10.3389/fmats.2022.991018

Engineered electrospun poly(lactic-co-glycolic acid)/Si_3N_4 nanofiber scaffold promotes osteogenesis of mesenchymal stem cell

Changsong Zhou[1], Shenghui Su[1]*, Jiwen Fan[2], Jiuzao Lin[1]* and Xiaoyong Wang[1]*

[1]Department of Orthopaedics, Ningde Municipal Hospital of Ningde Normal University, Ningde, Fujian, China, [2]Department of Orthopaedics, Nanfang Hospital, Southern Medical University, Guangzhou, China

Nanofibers show promise as bone tissue engineering scaffolds (BTESs). In this study, electrospun poly (lactic-co-glycolic acid) (PLGA)/silicon nitride (Si_3N_4) composite nanofiber membranes were formed and the osteogenesis capability of mesenchymal stem cells (MSC) from the scaffold marrow was investigated. By modifying the different properties of Si_3N_4 in the PLGA, two hybrid scaffolds were successfully prepared, including the PLGA/Si_3N_4 (1 wt.%) nanofiber scaffold and PLGA/Si_3N_4 (2 wt.%) nanofiber scaffold. The diameter of the fiber nanofiber scaffold PLGA/Si_3N_4 was decreased and the mechanical strength was increased compared to PLGA. *In vitro* studies showed better cell adhesion and proliferation on the PLGA/Si_3N_4 nanofiber scaffold compared to the PLGA nanofiber scaffold. The integration of Si_3N_4 promoted osteogenesis capacity by increasing the gene expression of bone-related proteins (BMP2, ALP, OPN, COL1a1, Runx2, and OCN), calcium deposits, and support of ALP activity compared to those for the PLGA nanofiber scaffold. Similarly, the PLGA/Si_3N_4 (2 wt.%) nanofiber scaffold showed better mechanics and biological activity compared to the PLGA/Si_3N_4 (1 wt.%) nanofiber scaffold. Overall, the PLGA/Si_3N_4 nanofiber scaffold showed potential as a promising hybrid scaffold for bone regeneration.

KEYWORDS

electrospinning, PLGA, Si_3N_4, bone tissue engineering scaffold, MSCs

Introduction

The demand is large for a graft or bone substitute to heal bone defects resulting from trauma, bone infections, osteomyelitis, necrosis, and tumors. BTES have been used as bone graft substitutes and overcome the limitations of all-/autografts.

From perspectives of developmental biology and tissue regeneration, an ideal BTES is designed by considering the following aspects: appropriate mechanical strength,

biological signaling factors, biomimetic structure, and selection of proper cell lineage (Lopes et al., 2018).

Natural and synthetic polymers with good biocompatibility are commonly used in the construction of BTES (Bharadwaz and Jayasuriya, 2020). While flexibility in processing and stability in artificial and mechanical strength are some advantages of synthetic polymers, they may lead to weak immune responses (Tamayol et al., 2013). Synthetic polymers such as polycaprolactone (PCL) (Heydari et al., 2017), poly (glycolic acid) (PGA) (Telemeco et al., 2005), poly (lactic-co-glycolic acid) (PLGA) (Loureiro et al., 2020), polyhydroxybutyrate (PHB) (Zhou et al., 2017), poly (propylene fumarate) (PPF) (Diez-Pascual and Diez-Vicente, 2017), and polycaprolactone (PLGA) show high-level mechanical properties (Bose et al., 2012). PLGA additionally shows high compatibility, as well as good biodegradability, chemical stability, thermal stability, nontoxicity, and histocompatibility and is widely used in the production and processing of drug carriers and tissue engineering scaffolds, and for wound healing [10]. The hydrophobic surface of PLGA results from ester bonds and high molecular weight, which lead to decreased surface wettability, which is a challenge in scaffold construction (Miguel et al., 2018). In addition, the low mechanical strength of pure PLGA scaffolds limits its application in osteogenic repair (Ji et al., 2011). Different forms of PLGA, such as porous scaffolds, films, fibers, nanoparticles, and microspheres, have been designed to overcome these shortcomings (Bose et al., 2018); Compounding with other materials is also another method used for the optimization of this polymer (Turnbull et al., 2018).

The most common fillers in BTES are bioactive glass (Turnbull et al., 2018), ceramic, and nanosheet materials such as Laponite, black phosphorus, graphene, and oxide. Compared to other organic 2D sheet materials, the covalent Si-N bonds of Si_3N_4 show cleavage. A silicon-rich layer is formed on the substrate surface, promoting hydroxyapatite formation and hydroxyapatite cell adhesion like bioactive glass. This method produces bioactive materials with the strongest known osseointegration ability (Zanocco et al., 2019). Moreover, the nitrogen released from Si_3N_4 plays a fundamental role in stimulating bone[21] and also provides an antibacterial effect (Boschetto et al., 2020). The angiogenic and osteogenic activities of silicon ions have also been widely reported. Multiscale porous structures could provide enhanced protein adsorption (Zhu et al., 2017), regulation of cell behavior related to osteogenic differentiation (Kim et al., 2017), and vascular ingrowth, which is the precursor and basis for bone formation (Stegen et al., 2015). Electrospinning is a more effective and advantageous method to manage the final unique structures and properties of scaffolds compared to 3D printing and other traditional methods (Jun et al., 2018).

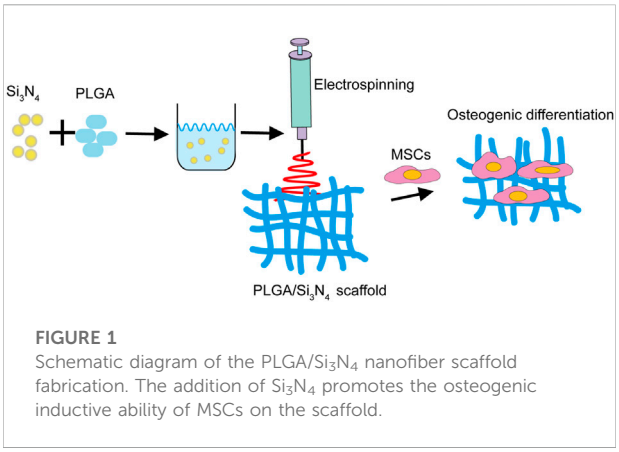

FIGURE 1
Schematic diagram of the PLGA/Si_3N_4 nanofiber scaffold fabrication. The addition of Si_3N_4 promotes the osteogenic inductive ability of MSCs on the scaffold.

Based on the excellent osteogenic regeneration potential of Si_3N_4, this study fabricated a novel composite scaffold doped with PLGA and Si_3N_4 by electrospinning (Figure 1). This work aimed to integrate the desired properties of PLGA and Si_3N_4 in a nanofiber scaffold. The surface topography, mechanical characteristics, and bioactivity of the scaffolds were examined by SEM, tension test, and MTT assay. This nanofiber scaffold may contribute to improved bone regeneration.

Materials and methods

Fabrication of PLGA/Si_3N_4 scaffolds

The desired amount of PLGA (240 mg) was dissolved in 2 ml of hexafluoroisopropanol (HFIP, Macklin, China) solvent and stirred for 24 h. Separately, Si_3N_4 (20–50nm, XFnano, China) particle powders were well dispersed in HFIP solvent. The two solutions were mixed by stirring for 24 h. The concentration of PLGA in HFIP was 12% w/v, while the Si_3N_4 amounts varied according to PLGA. The scaffolds were constructed on an electrospinning machine (YFSP-T, Yunfan (Tianjin) Instrument Co., Ltd., China). Finally, PLGA, PLGA/Si_3N_4 (1 wt.%), and PLGA/Si_3N_4(2 wt.%) nanofiber scaffolds were fabricated.

Characterization of the nanofiber scaffolds

A scanning electron microscope (SEM, Zeiss, Axiovert 200, Germany) was used to assess the morphology of the electrospun PLGA, PLGA/Si_3N_4 (1 wt.%), and PLGA/Si_3N_4

TABLE 1 Primers used for the qRT-PCR analysis.

Gene	Forward primer	Reverse primer
GAPDH	TCCAGTATGACTCTACCCACG	CACGACATACTCAGCACCAG
BMP2	TGCTCAGCTTCCATCACGAA	AATTTTGAGCTGGCTGTGGC
OPN	CCAGCCAAGGACCAACTACA	CCAAGTGGCTACAGCATCTGA
COL1a1	GATCCTGCCGATGTCGCTAT	GGGACTTCTTGAGGTTGCCA
OCN	GGCGCTACCTCAACAATGGA	GGCAACACATGCCCTAAACG
ALP	GTTACAAGGTGGTGGACGGT	ACAGTGGTCAAGGTTGGCTC
Runx2	GTGGCCAGGTTCAACGATCT	TGAGGAATGCGCCCTAAATCA

(2 wt.%) nanofiber scaffolds. All scaffolds were analyzed by SEM sputtered with a gold layer. Additionally, 30 pieces from each group were cached to calculate fiber diameters by using Image J pro.

The mechanical properties of the PLGA, PLGA/Si_3N_4 (1 wt.%), and PLGA/Si_3N_4 (2 wt.%) nanofiber scaffold were characterized using the same sample size (30 × 10 mm^2). The mechanical properties were assessed using a universal mechanical testing machine (Instron 68SC-05, United States) at a crosshead speed of 1.5 mm/min.

Cytocompatibility assessment of MSCs

Marrow mesenchymal stem cells (MSCs) were cultured on the different scaffolds marked as control, PLGA nanofiber scaffold, PLGA/Si_3N_4 (1 wt.%) nanofiber scaffold, and PLGA/Si_3N_4 (2 wt.%) nanofiber scaffold for 3 days. The MTT assay (Sigma-Aldrich, United States) was used to evaluate MSC proliferation after cell seeding on the scaffolds and without a scaffold (control).

After the MSCs were cultured on the PLGA, PLGA/Si_3N_4 (1 wt.%), and PLGA/Si_3N_4 (2 wt.%) nanofiber scaffolds for 3 days, the MSCs-nanofiber scaffolds were incubated with 1 μM calcein-AM and 1 μM PI for 30 min while protected from light. After washing three times with phosphate-buffered saline (PBS), images of cell morphology and cell interaction with the nanofiber scaffold in each group were captured using a fluorescence imaging microscope (Zeiss, Axiovert 200, Germany).

Gene expression

After the MSCs were cultured on the Control and PLGA, PLGA/Si_3N_4 (1 wt.%), and PLGA/Si_3N_4 (2 wt.%) nanofiber scaffolds for 3, 7, and 14 days, real-time qPCR (qRT-qPCR) was performed. The primers for these are shown in Table 1.

Alkaline phosphatase activity assay

After the MSCs were cultured on the Control and PLGA, PLGA/Si_3N_4 (1 wt.%), and PLGA/Si_3N_4 (2 wt.%) nanofiber scaffolds for 7 days, alkaline phosphatase activity (ALP) was measured as previously described (Solarbio, China) (Yin et al., 2011).

Alizarin red S staining

After the MSCs were cultured on the Control and PLGA, PLGA/Si_3N_4 (1 wt.%), and PLGA/Si_3N_4 (2 wt.%) nanofiber scaffolds for 7 days, ARS (Sigma-Aldrich, United States) staining was performed.

Statistical analysis

One-way analysis of variances (ANOVA) was used to compare more than two groups. Quantitative data were expressed as mean ± SD, with $^{*}p < 0.05$, $^{**}p < 0.01$, and $^{***}p < 0.001$ considered statistically significant.

Results and discussion

Characterization of the nanofiber scaffolds

The microstructures of the PLGA, PLGA/Si_3N_4 (1 wt.%), and PLGA/Si_3N_4 (2 wt.%) nanofiber scaffolds were observed by SEM, as shown in Figure 2. The addition of Si_3N_4 made the nanofiber scaffolds more uniform in size (Figure 2A). The diameter of pure PLGA nanofiber scaffold fibers ranged from 200 to 900 nm, with an average diameter of 429.3 ± 136.7 nm (Figures 2B,C). The composite PLGA/Si_3N_4 (1 wt.%) nanofiber scaffold showed a fiber diameter of around 100–500 nm, with an average diameter of 268.2 ± 66.7 nm. The further increase of Si_3N_4 up to 2 wt.% in the

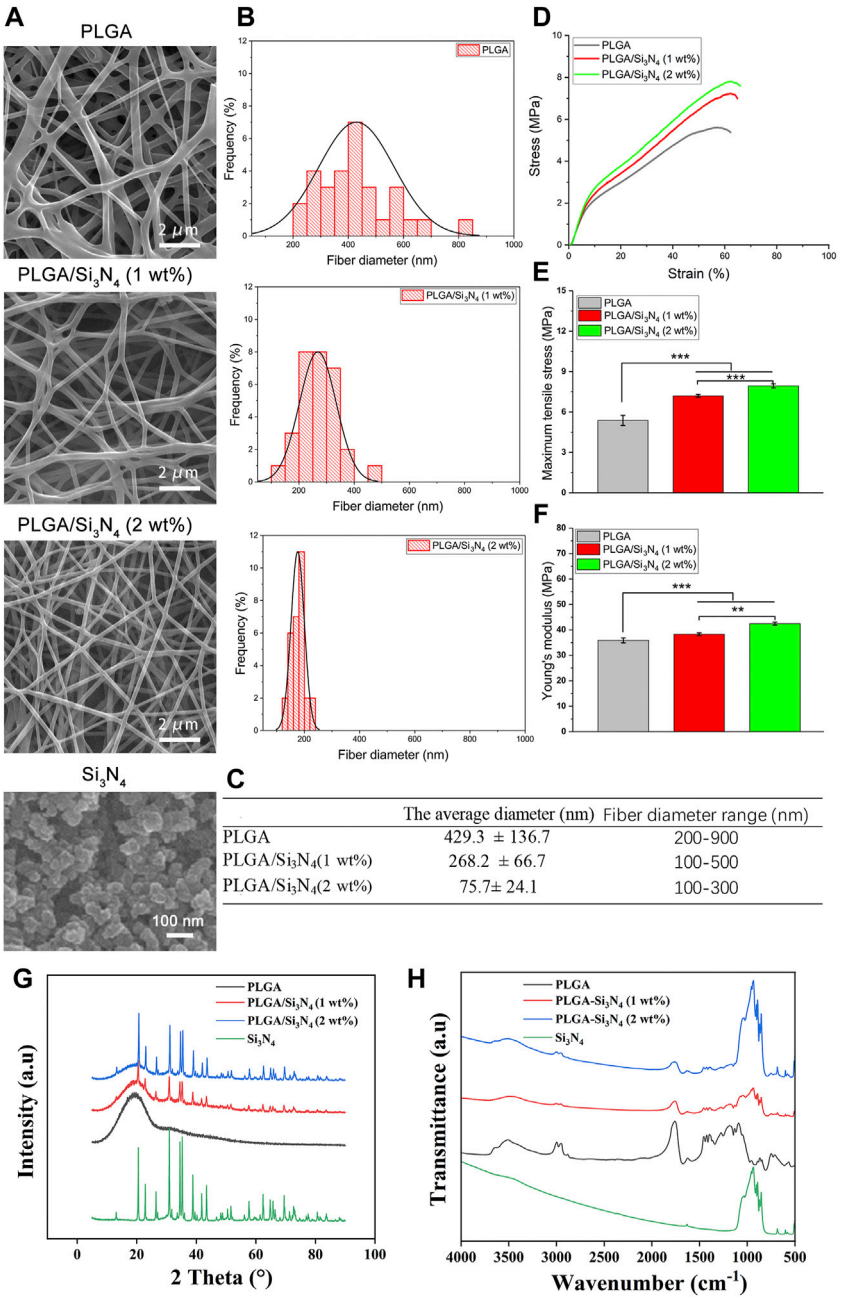

FIGURE 2
Characterization of the PLGA nanofiber scaffold, PLGA/Si_3N_4(1 wt.%) nanofiber scaffold, and PLGA/Si_3N_4 (2 wt.%) nanofiber scaffold. **(A)** SEM images of the electrospinning fibrous scaffolds and Si_3N_4. Scale bar: 2000 nm. **(B)** distribution of fiber diameters in the nanofiber scaffolds. **(C)** average fiber diameter of the nanofiber scaffolds. **(D)** typical tensile stress-strain curves of the nanofiber scaffolds. **(E)** maximum tensile stress of the nanofiber scaffolds. **(F)** Young's modulus of the nanofiber scaffolds. **(G)** XRD and **(H)** FTIR results for different groups of Si_3N_4, PLGA, PLGA/Si_3N_4 (1 wt.%), and PLGA/Si_3N_4 (2 wt.%).

PLGA/Si_3N_4 (1 wt.%) nanofiber scaffold decreased the range of fibers to 100–300 nm, with an average diameter of 175.7 ± 24.1 nm. Compared to the PLGA nanofiber scaffold and PLGA/Si_3N_4 (1 wt.%) nanofiber scaffold, the PLGA/Si_3N_4 (2 wt.%) nanofiber scaffold showed a smaller average diameter.

The stress-stress curves for the PLGA, PLGA/Si_3N_4 (1 wt.%), and PLGA/Si_3N_4 (2 wt.%) nanofiber scaffolds are shown in Figure 2D. The mechanical properties of the scaffolds are shown in Figures 2E,F. In the case of PLGA nanofiber scaffolds, the average maximum tensile strength and tensile modulus were 5.38 ± 0.37

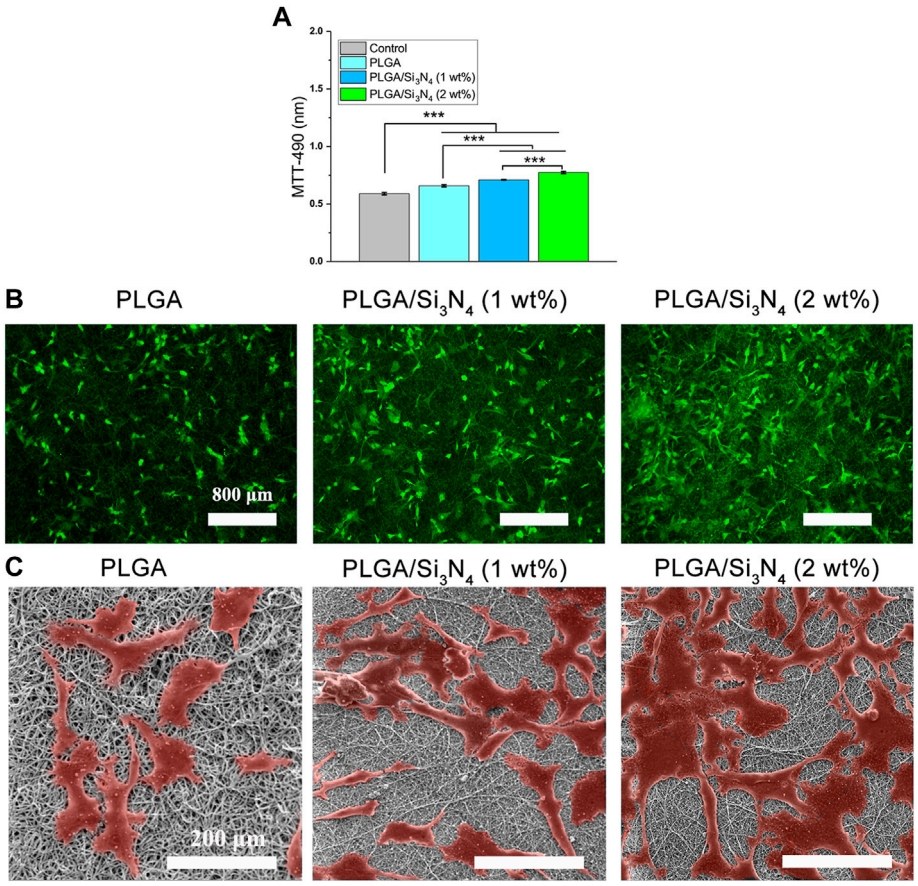

FIGURE 3
Control, PLGA nanofiber scaffold, PLGA/Si_3N_4 (1 wt.%) nanofiber scaffold, and PLGA/Si_3N_4 (2 wt.%) nanofiber scaffold cultured with MSCs for 3 days. **(A)** MTT assay results. **(B)** calcein-AM/PI stained for cell viability. scale bar: 800 μm. **(C)** SEM results. Scale bar: 200 μm.

(MPa) and 35.86 ± 0.95 (MPa), respectively. At 1 wt.% and 2 wt.% of Si_3N_4, the average final tensile strength significantly increased to 7.19 ± 0.11 (MPa) and 7.94 ± 0.15 (MPa), respectively. The Young's modulus also significantly increased to 38.28 ± 0.52 (MPa) and 42.46 ± 0.57 (Mpa), respectively.

The mechanism by which inorganic nanoparticles enhance the polymer phase was summarized in a previous study (Li et al., 2018). Similarly, PLGA nanofiber scaffold chains combine on the surface of Si_3N_4, producing more loops, tails, and strands. As a result, the fiber diameter of the PLGA/Si_3N_4 nanofiber scaffolds decreased with increasing Si_3N_4 content. A higher mechanical strength of the periosteum is more favorable for the osteogenic differentiation of BMSCs (Yang et al., 2021). Compared to smooth surfaces, the rougher surfaces of the PLGA/Si_3N_4 nanofiber scaffolds were favorable for osteogenic differentiation of bone marrow mesenchymal stem cells. Finally, interconnected porosity with an adequate pore size benefits the diffusion of growth factors, cells, oxygen, and nutrients and the exchange of waste products throughout the scaffold.

The results of XRD and FTIR showed that Si_3N_4 was compounded into the PLGA matrix. The mainly XRD diffraction peaks of Si_3N_4 appeared clearly in the Si_3N_4, PLGA/Si_3N_4 (1 wt.%), and PLGA/ Si_3N_4 (2 wt.%) groups, while PLGA showed amorphous peaks from 20° to 30°. Regarding the FTIR of Si_3N_4, the absorption peak of the Si-N bond is in the range of 800–1100 cm^{-1} while 1631 cm^{-1} is the shear vibration of -NH. Regarding the FTIR of PLGA, the absorption peaks at 2954 cm^{-1} and 2923 cm^{-1} are caused by the stretching vibrations of methyl and methylene, while the strong absorption peaks at 1759, 1182, and 1132 cm^{-1} represent the stretching vibrations of C=O, C-O-C, and C-O bonds, respectively. Most of the characteristic peaks from different materials were displayed on PLGA/Si_3N_4 (1 wt.%) and PLGA/ Si_3N_4 (2 wt.%), as in XRD, which proved the addition of Si_3N_4 to the PLGA matrix.

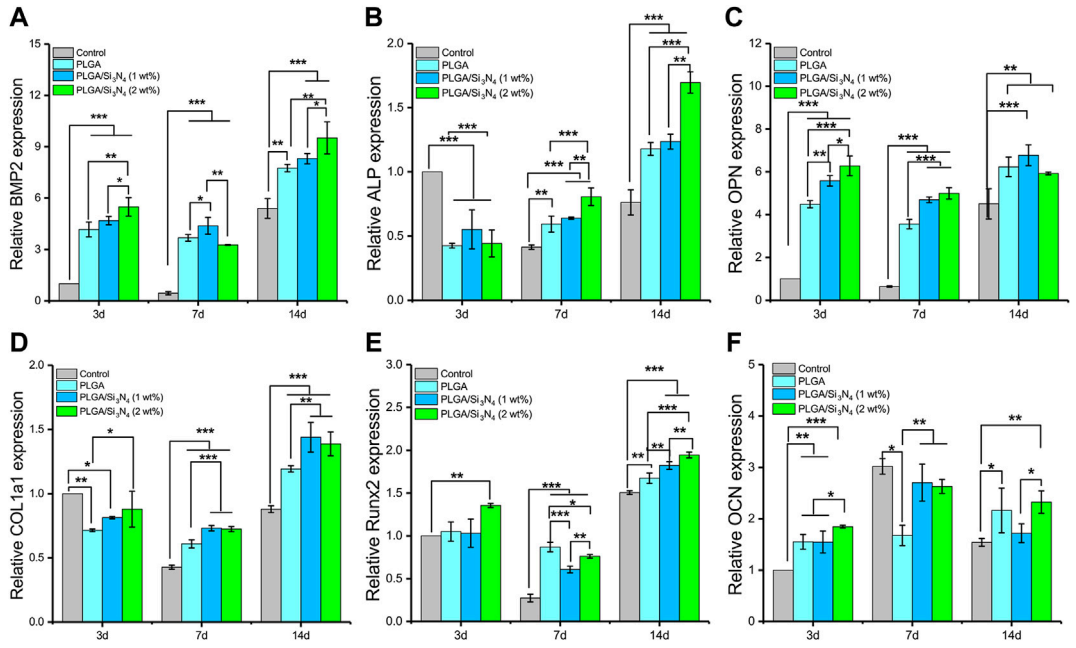

FIGURE 4
Gene expression of MSCs cultured on the PLGA nanofiber scaffold, PLGA/Si_3N_4 (1 wt.%) nanofiber scaffold, and PLGA/Si_3N_4 (2 wt.%) nanofiber scaffold for 3, 7, and 14 days. **(A)** *BMP2* expression. **(B)** *ALP* expression. **(C)** *OPN* expression. **(D)** *COL1a1* expression. **(E)** *Runx2* expression. **(F)** *OCN* expression.

Biocompatibility of the nanofiber scaffolds

To verify cell proliferation and cytotoxicity of the nanofiber, the cell viability on the scaffolds was assessed by MTT assay. As shown in Figure 3A, a higher number of live cells was observed on the PLGA/Si_3N_4 (2 wt.%) scaffold compared to those on the pure PLGA and PLGA/Si_3N_4 (1 wt.%) scaffolds.

The results of staining to assess the viability of MSCs using live and dead cells are shown in Figure 3B. More surviving cells were observed on the PLGA/Si_3N_4 nanofiber scaffolds. A slightly higher number of cells was present on the PLGA/Si_3N_4 (2 wt.%) nanofiber scaffold compared to the PLGA/Si_3N_4 (1 wt.%) nanofiber scaffold. Moreover, the MSCs on the PLGA/Si_3N_4 (2 wt.%) nanofiber scaffold showed abundant acicular tentacles, which indicated better cell adhesion. The results showed that the PLGA/Si_3N_4 (2 wt.%) nanofiber scaffold effectively supported MSC proliferation.

In vitro cellular responses including cell morphology and spreading are shown in Figure 3C. The PLGA matrix surfaces showed fewer cells compared to the PLGA/Si_3N_4 nanofiber scaffolds, likely due to the hydrophobic surface of the PLGA nanofiber scaffold. The overall cell morphology could be profoundly influenced by the micro-scale patterns (Rahmati et al., 2020). Several cells that were more spread out were observed on the PLGA/Si_3N_4 (1 wt.%) nanofiber scaffold. Higher numbers of adherent and spreading cells were observed on the PLGA/Si_3N_4 (2 wt.%) nanofiber scaffold due to the additional Si_3N_4.

PLGA/Si_3N_4 nanofiber scaffolds showed good biocompatibility and supported MSC adhesion, as shown by the results of the MTT assays, calcein-AM/PI staining, and SEM (Figure 3). Increased Si_3N_4 in the scaffold showed better effects on supporting cell growth, as demonstrated by the higher OD value of PLGA/Si_3N_4 (2 wt.%) nanofiber scaffold compared to that for the PLGA/Si_3N_4 (1 wt.%) nanofiber scaffold. The biocompatibility of silicon nitride has been established since the late 1980s. Three months after the implantation of silicon nitride ceramics into the bone marrow cavity of the rabbit femur, no inflammatory reaction in the tissue around the implant was observed (Howlett et al., 1989). Based on these results, scaffolds consisting of Si_3N_4 could enable efficient cell adhesion and proliferation.

Enhanced osteogenic differentiation by PLGA/Si_3N_4 *in vitro*

To evaluate the effect of Si_3N_4 nanoparticles on promoting osteogenic differentiation, qRT-PCR was performed to

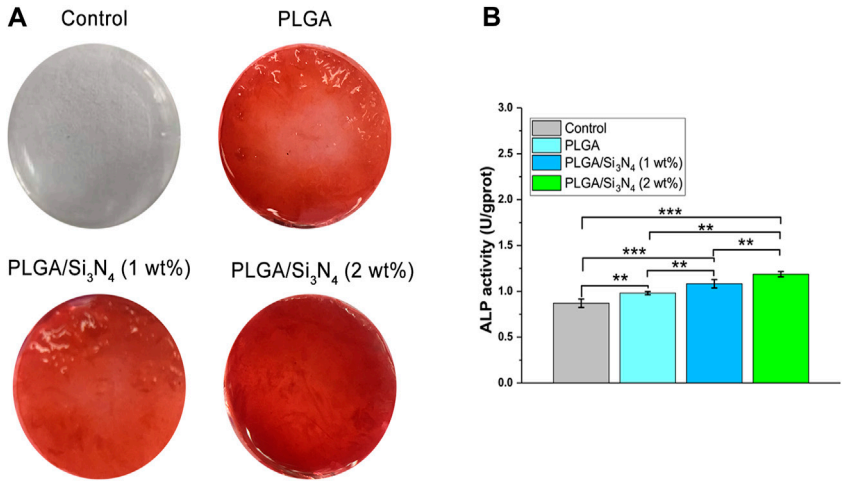

FIGURE 5
Nanofiber scaffolds supported osteogenic differentiation. **(A)** ARS staining of the nanofiber scaffolds at 7 days. The ARS solution stains calcium deposits red, with darker red indicating more calcium deposits. **(B)** ALP activity assay at 7 days for the nanofiber scaffold, PLGA/Si_3N_4 (1 wt.%) nanofiber scaffold, and PLGA/Si_3N_4(2 wt.%) nanofiber scaffold.

determine the gene expression levels of *BMP2*, *ALP, OPN, COL1a1, Runx2*, and *OCN*. PLGA/Si_3N_4 (1 wt.%) and PLGA/Si_3N_4 (2 wt.%) showed increased gene expression levels compared to those in PLGA (Figure 4). With the addition of a higher Si_3N_4 dose (2 wt.%), the nanofiber scaffold showed higher expression levels of osteogenic markers compared to a lower Si_3N_4 dose (1 wt.%). More specifically, as shown in Figure 4, PLGA/Si_3N_4 with 1 wt.% and 2 wt.% showed higher gene expression levels of *BMP2* (on days 3 and 14), *ALP* (on days 7 and 14), *OPN* (on days 3 and 7), *COL1a1* (on days 3 and 14), *Runx2* (on day 14), and *OCN* (on day 3). PLGA/Si_3N_4 (1 wt.%) showed higher gene expression levels than those in PLGA for *BMP2* (days 3 and 14), *ALP* (days 7 and 14), *OPN* (days 3 and 7), *COL1a1* (day 3), *Runx2* (day 14), and *OCN* (day 14). PLGA/Si_3N_4 (2 wt.%) had higher gene expression levels than those in PLGA for *BMP2* (days 3 and 14), *ALP* (days 7 and 14), *OPN* (days 3 and 7), *COL1a1* (days 3, 7, and 14), *Runx2* (days 3 and 14), and *OCN* (days 3, 7, and 14). Overall, PLGA/Si_3N_4 (2 wt.%) showed a nearly 2-fold increase in *BMP2* expression, 3.1-fold in *ALP*, 1.4-fold in *OPN*, 1.5-fold in *COL1a1*, 0.6-fold in *Runx2*, and 1.9-fold in *OCN* to 14 days. Overall, PLGA containing Si_3N_4 (1 wt.%) and Si_3N_4 (2 wt.%) significantly supported the gene expression of bone-related proteins.

In addition, the PLGA/Si_3N_4 scaffold osteogenic performance was assessed according to mineralization measured by ARS (Figure 5A) and ALP activity (Figure 5B). On the seventh day, the PLGA/Si_3N_4 (1 wt.%) nanofiber membrane gradually showed deeper ARS staining compared to that in the PLGA nanofiber membrane. With an increase in Si_3N_4 from 1 wt.% to 2 wt.%, the PLGA/Si_3N_4 (2 wt.%) nanofiber membrane showed the darkest red and most calcium nodes in MSC. ARS staining increased with increased Si_3N_4 concentration, suggesting that Si_3N may support the formation of calcium nodes. Additionally, the ALP activity was consistent with the results of alizarine red staining. Compared to the PLGA nanofiber membrane, ALP activity increased from 1 wt.% to 2 wt.% Si_3N_4, with the PLGA/Si_3N_4 (2 wt.%) nanofiber membrane showing the highest ALP activity. PLGA/Si_3N_4 (2 wt.%) also stimulated higher levels of *in vitro* mineralization compared to PLGA/Si_3N_4 (1 wt.%).

As a regulated molecule in osteogenic differentiation, BMP2 plays important roles in the whole process of endochondral ossification (Peng et al., 2005). The addition of Si_3N_4 can significantly promote the autocrine and paracrine signals of BMP2 to promote osteogenesis. Furthermore, bone formation and regeneration is a complex multi-factor process, in which transcription factors are important influencing factors. High expression of active ALP and RUNX2 indicates osteoblast differentiation into mature osteocytes (Chen et al., 2016). As the Si_3N_4 content increased, the expression of osteogenic promoter genes significantly increased, thus demonstrating the ability of Si_3N_4 to promote osteogenesis. Similarly, the expression and maintenance of the extracellular matrix are also important signals for BMSCs in osteogenic differentiation. During long-term culture (14 days), *COL1a1* and *OCN* expression levels were significantly higher in PLGA/Si_3N_4 (2 wt.%) nanofiber scaffolds compared to the levels in the other scaffolds.

The control showed hardly any ARS coloring, while each composite membrane showed bright red coloring. Among them, PLGA/Si_3N_4 nanofiber scaffold (2 wt.%) showed the deepest red due to an appropriate osteogenic mechanical microenvironment. These results validate the osteogenic effects of PLGA/Si_3N_4 electrospun films.

Conclusion

This study successfully manufactured a Si_3N_4-integrated PLGA nanofiber scaffold using the electrospinning technique. This scaffold showed good biological and mechanical properties. The Si_3N_4 nanoparticle composition significantly facilitated osteogenic differentiation and mineralization of MSCs *in vitro* based on different Si_3N_4 content, revealing the role of Si_3N_4 in electrospun nanofiber scaffolds. These results verify the potential of PLGA/Si_3N_4 scaffolds for BTES.

Data availability statement

The original contributions presented in the study are included in the article/supplementary material; further inquiries can be directed to the corresponding authors.

Author contributions

Conceptualization, CZ; methodology, CZ and SS; formal analysis, SS and JL; data curation, CZ and JF; writing-original draft preparation, CZ; writing-review and editing, JL and XW.

Funding

This study was supported by the Scientific Research Project of Medical Technology Improvement of Ningde Health Committee, Fujian Province, China (Grant number: 2020003).

Conflict of interest

The authors declare that the research was conducted in the absence of any commercial or financial relationships that could be construed as a potential conflict of interest.

Publisher's note

All claims expressed in this article are solely those of the authors and do not necessarily represent those of their affiliated organizations, or those of the publisher, the editors, and the reviewers. Any product that may be evaluated in this article, or claim that may be made by its manufacturer, is not guaranteed or endorsed by the publisher.

References

Bharadwaz, A., and Jayasuriya, A. C. (2020). Recent trends in the application of widely used natural and synthetic polymer nanocomposites in bone tissue regeneration. *Mater. Sci. Eng. C* 110, 110698. doi:10.1016/j.msec.2020.110698

Boschetto, F., Marin, E., Ohgitani, E., Adachi, T., Zanocco, M., Horiguchi, S., et al. (2020). Surface functionalization of PEEK with silicon nitride. *Biomed. Mat.* 16, 015015. doi:10.1088/1748-605x/abb6b1

Bose, S., Ke, D., Sahasrabudhe, H., and Bandyopadhyay, A. (2018). Additive manufacturing of biomaterials. *Prog. Mat. Sci.* 93, 45–111. doi:10.1016/j.pmatsci.2017.08.003

Bose, S., Roy, M., and Bandyopadhyay, A. (2012). Recent advances in bone tissue engineering scaffolds. *Trends Biotechnol.* 30, 546–554. doi:10.1016/j.tibtech.2012.07.005

Chen, Q., Shou, P., Zheng, C., Jiang, M., Cao, G., Yang, Q., et al. (2016). Fate decision of mesenchymal stem cells: Adipocytes or osteoblasts? *Cell Death Differ.* 23, 1128–1139. doi:10.1038/cdd.2015.168

Diez-Pascual, A. M., and Diez-Vicente, A. L. (2017). Multifunctional poly(glycolic acid-co-propylene fumarate) electrospun fibers reinforced with graphene oxide and hydroxyapatite nanorods. *J. Mat. Chem. B* 5, 4084–4096. doi:10.1039/c7tb00497d

Heydari, Z., Mohebbi-Kalhori, D., and Afarani, M. S. (2017). Engineered electrospun polycaprolactone (PCL)/octacalcium phosphate (OCP) scaffold for bone tissue engineering. *Mater. Sci. Eng. C* 81, 127–132. doi:10.1016/j.msec.2017.07.041

Howlett, C. R., McCartney, E., and Ching, W. (1989). The effect of silicon nitride ceramic on rabbit skeletal cells and tissue. An *in vitro* and *in vivo* investigation. *Clin. Orthop. Relat. Res.* 244, 293–304. doi:10.1097/00003086-198907000-00032

Ji, W., Sun, Y., Yang, F., van den Beucken, J. J., Fan, M., Chen, Z., et al. (2011). Bioactive electrospun scaffolds delivering growth factors and genes for tissue engineering applications. *Pharm. Res.* 28, 1259–1272. doi:10.1007/s11095-010-0320-6

Jun, I., Han, H. S., Edwards, J. R., and Jeon, H. (2018). Electrospun fibrous scaffolds for tissue engineering: Viewpoints on architecture and fabrication. *Int. J. Mol. Sci.* 19, 745. doi:10.3390/ijms19030745

Kim, J. J., El-Fiqi, A., and Kim, H. W. (2017). Synergetic cues of bioactive nanoparticles and nanofibrous structure in bone scaffolds to stimulate osteogenesis and angiogenesis. *ACS Appl. Mat. Interfaces* 9, 2059–2073. doi:10.1021/acsami.6b12089

Li, A., Jia, Y., Sun, S., Xu, Y., Minsky, B. B., Stuart, M. A. C., et al. (2018). Mineral-enhanced polyacrylic acid hydrogel as an oyster-inspired organic-inorganic hybrid adhesive. *ACS Appl. Mat. Interfaces* 10, 10471–10479. doi:10.1021/acsami.8b01082

Lopes, D. L., Martins-Cruz, C., Oliveira, M. B., and Mano, J. F. (2018). Bone physiology as inspiration for tissue regenerative therapies. *Biomaterials* 9, 240–275. doi:10.1016/j.biomaterials.2018.09.028

Loureiro, J., Torres, A. L., Neto, T., Aguiar, P., Barrias, C. C., Pinto, M. T., et al. (2020). Corrigendum to "Conjugation of the T1 sequence from CCN1 to fibrin hydrogels for therapeutic vascularization" [Mater. Sci. & Eng. C. 104 (2019) 109847]. *Mater. Sci. Eng. C* 108, 110514. doi:10.1016/j.msec.2019.110514

Miguel, S. P., Figueira, D. R., Simoes, D., Ribeiro, M. P., Coutinho, P., Ferreira, P., et al. (2018). Electrospun polymeric nanofibres as wound dressings: A review. *Colloids Surfaces B Biointerfaces* 169, 60–71. doi:10.1016/j.colsurfb.2018.05.011

Peng, H., Usas, A., Olshanski, A., Ho, A. M., Gearhart, B., Cooper, G. M., et al. (2005). VEGF improves, whereas sFlt1 inhibits, BMP2-induced bone formation and bone healing through modulation of angiogenesis. *J. Bone Min. Res.* 20, 2017–2027. doi:10.1359/jbmr.050708

Rahmati, M., Silva, E. A., Reseland, J. E., and Haugen, H. J. (2020). Biological responses to physicochemical properties of biomaterial surface. *Chem. Soc. Rev.* 49, 5178–5224. doi:10.1039/d0cs00103a

Stegen, S., van Gastel, N., and Carmeliet, G. (2015). Bringing new life to damaged bone: The importance of angiogenesis in bone repair and regeneration. *Bone* 70, 19–27. doi:10.1016/j.bone.2014.09.017

Tamayol, A., Akbari, M., Annabi, N., Paul, A., Khademhosseini, A., and Juncker, D. (2013). Fiber-based tissue engineering: Progress, challenges, and opportunities. *Biotechnol. Adv.* 31, 669–687. doi:10.1016/j.biotechadv.2012.11.007

Telemeco, T. A., Ayres, C., Bowlin, G. L., Wnek, G. E., Boland, E. D., Cohen, N., et al. (2005). Regulation of cellular infiltration into tissue engineering scaffolds composed of submicron diameter fibrils produced by electrospinning. *Acta Biomater.* 1, 377–385. doi:10.1016/j.actbio.2005.04.006

Turnbull, G., Clarke, J., Picard, F., Riches, P., Jia, L., Han, F., et al. (2018). 3D bioactive composite scaffolds for bone tissue engineering. *Bioact. Mat.* 3, 278–314. doi:10.1016/j.bioactmat.2017.10.001

Yang, G., Liu, H., Cui, Y., Li, J., Zhou, X., Wang, N., et al. (2021). Bioinspired membrane provides periosteum-mimetic microenvironment for accelerating vascularized bone regeneration. *Biomaterials* 268, 120561. doi:10.1016/j.biomaterials.2020.120561

Yin, G., Huang, Z., Deng, M., Zeng, J., and Gu, J. (2011). Preparation and cell response of bio-mineralized Fe3O4 nanoparticles. *J. Colloid Interface Sci.* 363, 393–402. doi:10.1016/j.jcis.2011.07.009

Zanocco, M., Marin, E., Rondinella, A., Boschetto, F., Horiguchi, S., Zhu, W., et al. (2019). The role of nitrogen off-stoichiometry in the osteogenic behavior of silicon nitride bioceramics. *Mater. Sci. Eng. C* 105, 110053. doi:10.1016/j.msec.2019.110053

Zhou, T., Li, G., Lin, S., Tian, T., Ma, Q., Zhang, Q., et al. (2017). Electrospun poly(3-hydroxybutyrate-co-4-hydroxybutyrate)/graphene oxide scaffold: Enhanced properties and promoted *in vivo* bone repair in rats. *ACS Appl. Mat. Interfaces* 9, 42589–42600. doi:10.1021/acsami.7b14267

Zhu, K., Shin, S. R., van Kempen, T., Li, Y. C., Ponraj, V., Nasajpour, A., et al. (2017). Gold nanocomposite bioink for printing 3D cardiac constructs. *Adv. Funct. Mat.* 27, 1605352. doi:10.1002/adfm.201605352